Cement and Concrete Research 40 (2010) 1673–1680

Contents lists available at ScienceDirect

Cement and Concrete Research

journal homepage: http://ees.elsevier.com/CEMCON/default.asp

The effect of drying on early-age morphology of C–S–H as observed in environmental SEM

P.C. Fonseca [a,*], H.M. Jennings [a,b]

[a] Northwestern University, Department of Civil and Environmental Engineering, Evanston IL 60208, United States
[b] Northwestern University, Department of Materials Science and Engineering, Evanston IL 60208, United States

ARTICLE INFO

Article history:
Received 5 November 2008
Accepted 5 August 2010

Keywords:
A. morphology
A. mechanism
A. drying
A. humidity
B. calcium–silicate–hydrate (C–S–H)
B. microstructure
B. scanning electron microscopy (SEM)

ABSTRACT

The morphology of early-age C–S–H, often referred to as outer product or low-density C–S–H, is generally accepted to be fibrillar and forms mainly during the early stages of hydration. This paper reports the effect of drying on the microstructure in young tricalcium silicate paste, which provides insight into the mechanism that leads to the fibrillar morphology. During the first few days after C_3S is mixed with water, the morphology of C–S–H is more affected by drying rate than by relative humidity. This sensitivity is most apparent at partial pressures greater than 85%. During this time, the fibrillar C–S–H product can be suppressed by drying C_3S paste samples very slowly prior to imaging. This approach is interpreted as evidence that this fibrillar morphology, which naturally form over time, grow as tiny colloidal particles that rearrange during the early stages of hydration, leading to well-established larger scale morphologies.

1. Introduction and Background

The observed structure of calcium–silicate–hydrate (C–S–H) depends on scale. At the atomic scale, C–S–H is described as a disordered layered calcium silicate analogous to imperfect tobermorite, perhaps mixed with jennite [1]. At the nanoscale (1–100 nm), evidence suggests that C–S–H behaves like a colloidal precipitate with mechanical properties similar to a gel [2] [3]. The pores at this level are a mix of gel pores (typically classified as under 10 nm) and larger capillary pores.

The first physical characterization of C–S–H at several scales originated with Powers and Brownyard in the 1940s. They suggested the existence of inside and outside products to denote hydration products that lie inside and outside the clinker particles, respectively [4] [5]. The widely used terms inner product (IP) and outer product (OP), however, were coined by Taplin [6], who independently investigated hydration reactions in Portland cement. Although the transition between the IP and OP may not align with the original clinker boundary, this terminology has continued to be used by many researchers of cement microstructure.

The development of electron microscopy in the 1950s produced a vast array of observations of the morphology of C–S–H. By the early 1970s, Diamond used scanning electron microscopy (SEM) to describe four C–S–H morphologies observed in Portland cement paste [7]. These four types consist of three types of OP and one IP. Type I was described as fibrous particles that "seem to be partly-rolled sheets" ranging from 0.5 to 2 μm in length. The fibers appeared to be more abundant in younger pastes. Type II was a "reticular network" or "interlocking structure" seen in Portland cement pastes but not in C_3S or β-C_2S pastes. Type III was described as "relatively nondescript" or consisting of an "equant grain morphology", approximately 300 nm in diameter. Finally, the C–S–H that constituted IP found in older pastes was classified as Type IV.

Jennings *et al.* correlated these morphological features to its formation during specific hydration stages and further postulated that spatial restrictions also influence the resulting morphology [8]. More recently, Jennings and Tennis have introduced a model of colloidal particles that pack into two separate arrangements: 1) high-density (HD) product and 2) low-density (LD) product [9] [10]. Based on the Brunauer–Emmett–Teller (BET) surface area and small-angle neutron scattering (SANS) measurements, Jennings showed that the LD product forms during the main exotherm during the first or second day of hydration.

Since Diamond's C–S–H classification system, the literature has been replete with terminology for describing the physical characteristics of C–S–H, but the recent trend has been to move back to distinguishing two main forms [11]. Richardson and Groves, who used an impressive array of high-resolution transmission electron microscopy (TEM) images [12], prefer the IP and “OP " nomenclature [13]; Diamond and Bonen refer to phenograins and groundmass; and Jennings prefers the quantitative HD/LD terminology. Although these researchers agree that C–S–H is composed of two types of hydration

* Corresponding author. Tel.: +1 847 942 0196; fax: +1 847 491 4011.
E-mail addresses: illa@u.northwestern.edu (P.C. Fonseca), h-jennings@northwestern.edu (H.M. Jennings).

0008-8846/$ – see front matter © 2010 Elsevier Ltd. All rights reserved.
doi:10.1016/j.cemconres.2010.08.007

products, the nomenclature does not necessarily correlate with one another.

One familiar problem with electron microscopy is that specimen preparation is often harsh or damaging. It has been suggested that permanent changes occur due to drying or heating [14] [15]. Irreversible shrinkage occurs both at the macroscale (irreversible drying shrinkage) and at the micron scale [16]. Furthermore, experimental evidence indicates that drying changes the arrangement of nanoparticles in cement [17]. For example, Thomas *et al.* used SANS to analyze nanoscale effects of drying on saturated, dried, and resaturated Portland cement paste [18]. They showed that the total surface area decreased during first drying, which indicated a compaction of the C–S–H gel structure. Furthermore, specimens resaturated from 80% relative humidity (RH) recovered their surface area, whereas specimens dried below 80% RH did not. The latter case implies permanent restructuring of the cement nanostructure even when only slightly dried.

Gas sorption experiments suggest that, in addition to relative humidity, drying rate also causes microstructural changes to cement paste. To determine the surface area of C–S–H, Hunt took BET nitrogen sorption measurements of cement paste [19]. Isotherms from specimens dried prior to crushing were compared to isotherms of samples dried after crushing. The results showed that the measured surface areas were higher for the samples dried after crushing. Although not explicitly stated by Hunt, it has been concluded by researchers that, because crushed samples dry more rapidly than uncrushed samples, higher surface areas must have been a result of more rapid drying [20] [21]. This change in surface area suggests a change in the microstructure.

In a review of the structure of gels, Scherer asserts that, although C–S–H is a precipitate rather than a true gel, it exhibits gel-like characteristics at colloidal dimensions [2]. He noted that damage during drying is caused not by the magnitude of capillary pressure but by the gradient of the pressure, which causes differential shrinkage [22]. This gradient is dependent on the permeability of the material and the rate of evaporation. It follows that higher drying rates may cause more microstructural changes to C–S–H compared to lower drying rates. These changes are also likely to occur at high humidity levels [23].

At the microscopic level, much research has been directed to the problem of whether the aforementioned morphologies are artifacts. Since the 1970s, several experiments designed to eliminate sample desiccation during imaging have been performed. The earliest published work that characterizes wet C–S–H was reported by Double, who used a high-voltage environmental cell in a TEM [24] [25]. By sandwiching unhydrated cement particles between two thin plates and feeding water from a tiny inlet pipe, the development of hydration products could be observed *in situ*, which was interpreted in terms of reaction mechanisms that control the rate of hydration. After 1 day of hydration, significant fibrillar development similar to Diamond's Type I product was observed around the cement grain. The results imply that the fibers are part of the natural wet state of the OP. However, the samples were made of Portland cement, which produces fibrous ettringite. Furthermore, the samples contained high water content (w/c) and therefore were not representative of the w/c in typical concrete structures. Nitrogen BET measurements show that the surface area of C–S–H increases with w/c [19], indicating that the morphology of C–S–H is not fixed but, instead, adapts to its surroundings. It is therefore possible that fibrous C–S–H tends to form when more space is available.

Shortly after Double performed his high-voltage TEM (HVTEM) experiments, Jennings and Pratt used HVTEM with a gas-reaction cell (100% RH) to observe the C–S–H hydration product in hardened cement paste with realistic w/c [26]. In a 4-day-old cement paste that was wet cured at 50 °C with 0.5 w/c, they captured micrographs of C–S–H that show a sheetlike appearance in the wet state. As the sample dried (approximately 30 minutes), the sheets took on a needlelike appearance similar to the needles in Double's HVTEM observations. Further work [8] showed that much of the C–S–H product in the wet state appeared to be nondescript. Noting that the sheetlike appearance only occurred with very wet specimens, Jennings and Pratt postulated that the needles were likely an artifact of drying. This initial sheetlike appearance is one of the few direct observations of changes to C–S–H during drying.

Silva and Monteiro [27] [28] used soft X-ray transmission to observe fibrous hydration product as early as 22 minutes after mixing C_3S paste. Similar to the aforementioned Double's experiments, both these techniques require diluted samples unrepresentative of the conditions in concrete structures.

Cryomicroscopy is another method for observing the hydration of cement without the effects of drying. Zingg *et al.* [29] use cryomicroscopy to observe early hydration products of cement paste. At 6-minute hydration, tiny fibrous hydration products around larger ettringite crystals were observed on pastes that were well dispersed with superplasticizers. The formation of ice crystals was suppressed by lowering the temperature very quickly ($100-500^{\circ}C$ per second) at very high pressures (over 2000 bar). However, C–S–H is known to be sensitive to its surrounding environment, and the high dose of superplasticizers could have affected the C–S–H morphology.

One of the clearest sets of high-resolution cement paste micrographs was presented by Möser and Stark [30], who imaged fracture surfaces of hardened C_3S, β-C_2S, and Portland cement paste with realistic w/c using an environmental SEM (ESEM). They observed a needlelike product that lengthened with hydration time. To avoid desiccation, Möser and Stark broke the samples in the ESEM chamber using a micromanipulator. One shortcoming of their method is the assumption that all humidity levels higher than 80% moist are enough to prevent drying damage. As we will show, significant physical changes in C–S–H can be seen at 90% RH, and few changes are observed lower than 85% RH. Furthermore, we observe that the rate of drying, in particular between 100% and 85% RH, significantly affects the C–S–H morphology. If Möser and Stark subjected samples to partial pressures lower than 90%, drying may have altered the C–S–H microstructure.

The mechanisms that govern the formation of the different micron-scale morphologies are still largely mysterious. One of the most quoted possibilities is that the mechanisms are analogous to the reverse silicate garden, where needles grow as a membrane ruptures and that fluid containing high concentrations of ions enters the larger capillary space, resulting in the formation of hollow needles [31]. The problem is that confirmed hollow needles of C–S–H have not been observed. At the nanoscale, the LD structure has been associated with the agglomeration of 5-nm particles [32], but little is said about how this condition relates to the structure at the micron scale.

The thesis of this paper is that the different morpohologies, in particular the needles, are the result of dispersed or partially dispersed nanometric particles that precipitate and rearrange during the early days of reaction. The natural formation process can be interrupted by drying during the first few days, which provides evidence for this mechanism. The following experiments are the first to use an ESEM to observe the effect of drying rate on the morphology of C–S–H, with particular attention to high (greater than 80%) relative humidity. By comparing micrographs of hydrated C_3S pastes subjected to decreasing rates of drying, the open question of the mechanism of morphology development during the early reaction is revisited.

2. Experimental Method

For this experiment, fracture surfaces of C_3S paste samples at 3- and 21-day curing times were imaged. The surface area of the C_3S particles was 0.47 m^2/g (measured using SANS). Fracture surfaces

were chosen, because cutting and polishing would damage the fragile C–S–H product. Note that fracture occurs along weak zones with disproportionally higher porosity. Therefore, extra space may have been available for hydration product to form. However, because the curing time was constant among the samples for comparison, a direct comparison of the C–S–H morphology could be made.

The w/c for all samples was 0.5, each with approximately 1-mm thickness. The first four samples were wet cured for 3 days at room temperature prior to drying. This curing time was chosen to be at least 3 days, because younger specimens tended to suffer from beam damage. The fifth and sixth samples were wet cured for 21 days and dried at two different rates.

After curing, Samples 1–4 were subjected to progressively slower drying rates. Sample 1 was oven dried. Sample 2 was rapidly dried in the ESEM chamber to 33% RH at 5°C. The total drying time was approximately 2 minutes. Sample 3 was also dried in the ESEM at 5°C but over a 2-hour time span. Sample 4 was slowly dried in 3-day stages, for a total of 18 days, by progressively stepping the sample down in tightly sealed desiccators that contain 94%, 85%, 76%, 54%, 43%, and 33% RH at room temperature. Exposure to CO_2 was minimized by flushing each desiccator with nitrogen gas to prevent the formation of calcium carbonate. Although chemical analysis was not performed, no evidence of carbonation was observed. The pore water in the paste was allowed to equilibrate at each partial pressure before drying it further. Because hydration essentially ceases if the internal humidity level of cement paste is below 85% [33], the curing age of Sample 4 is considered to be 3 days. Sample 5 was wet cured for 21 days and then subjected to the same drying conditions as in Sample 2. Sample 6, also wet cured for 21 days, was incrementally dried using the same method as in Sample 4, but over a period of 4 days. A summary of the specimens is presented in Table 1.

The microscope used was an FEI Quanta Environmental ESEM with a Peltier stage to control the temperature at the base of the specimen. We used an accelerating voltage of 20 kV; higher voltages easily damaged the microstructure, whereas lower voltages tended to result in grainy images. The working distance was 7.0±0.1 mm. The RH was controlled by setting the Peltier stage at a low temperature, such as 5°C, and then specifying fractions of the saturated vapor pressure for that temperature. For example, if an 85% RH was desired at 5°C, the pressure was set to 0.85*(6.54 Torr) = 5.56 Torr.

In specimens that were not to be dried prior to imaging (such as Sample 3), care was taken to ensure that drying did not occur during the pump-down sequence. A few drops of distilled water were placed directly on and around the specimens, and the temperature was set a few minutes prior to pumping down. Purging of excess gasses consisted of pumping the chamber 8 to 10 times between 7 and 10 Torr at 4.8°C. During pump-down, we could see the bulk water on the specimen through a camera located in the chamber. If evaporation occurred, it was assumed that drying had occurred prior to imaging, and the specimen was discarded. Although early efforts to maintain saturation during the pump-down sequence failed, with practice, the results became successful and repeatable.

3. Results

3.1. Comparison of C–S–H morphology with various drying rates

The micrographs in Figs. 1–6 are representative of images taken at many locations on several hundred specimens. To avoid obscuring the microstructure, each sample was left uncoated. Some charging resulted at lower partial pressures, particularly in oven-dried specimens. Imaging at higher partial pressures (greater than 50%) tended to result in crisp well-defined images.

Fig. 1 is a micrograph of Sample 1, showing the morphology of C–S–H subjected to oven drying, the highest rate of drying in this experiment. Fine needles, approximately 16 nm thick and 500 nm long, are shown radiating outward from the center of individual C_3S particles. Note that, in this and all other samples, the dimensions are estimates taken with caution and are used to describe trends only.

Sample 2, which was rapidly dried to 33% RH in the ESEM, is shown in micrographs in Fig. 2. These images resemble Diamond's Type I product. In Fig. 2(a), a relatively low magnification image of C–S–H product is shown encasing many individual C_3S particles. Higher magnification in Fig. 2(b) illustrates fibrillar C–S–H in detail. The length of each fibril is about 2 μm, and the width is about 25 ± 5 nm.

Sample 3 was prepared in exactly the same manner as Sample 2, except that the partial pressure was slowly reduced from 100% to 33% over the course of 2 hours. Micrographs of the drying progression are shown in Fig. 3. The C–S–H product resembles a fibrillar morphology. These fibrils are thicker and are half as long as the needles in Sample 2. Based on this comparison, it is still not clear whether the microstructure in Fig. 3 is representative of the natural state of C–S–H. However, we can already deduce that the change in drying time altered the microstructure. In the case of Sample 2, the quicker drying time resulted in longer and thinner needles.

Sample 4 was dried in stages from 100% RH to 33% RH over the course of 18 days. The paste was then imaged at both 75% and 33% partial pressures. Fig. 4 shows micrographs of a markedly different microstructure. It is amorphous, and rather than producing long thin needles, a bumpy appearance is shown. These bumps tended to slightly elongate as the partial pressure was lowered to 33%, indicating that drying in the ESEM still had a mild effect on the microstructure. The bumps are significantly shorter and are at least twice as wide as the fibers in Sample 3, and they are roughly four times as wide as the fibrils in Sample 2.

Sample 5 was wet cured for 21 days before rapid drying in the ESEM (the same drying condition as in Sample 2). In Fig. 5, we see that the morphology of Sample 5 resembles that of Samples 1–3 but is very unlike Sample 4. These results indicate that the microstructure is less affected by the time after curing and is more affected by the rate of drying prior to imaging.

Sample 6 was also wet cured for 21 days but was subsequently dried from 100% RH to 75% RH in stages for 4 days after curing. As shown in Fig. 6, there is a mixed result in morphology, with about half the image presenting a fibrillar morphology, whereas the other half

Table 1
Summary of samples.

Sample number	Curing time (in days)	Drying method	Length of needles at 75% RH (nm)	Width of needles at 75% RH (nm)	Length of needles at 33% RH (nm)	Width of needles at 33% RH (nm)
1	3	Oven	-	-	500	16
2	3	Rapid (2 min)	-	-	1000	25
3	3	Slow (2 hours)	500	80	700	50
4	3	Incremental (18 days)	100–240	240	100–280	100
5	21	Rapid (2 min)	600	50	1000	40–50
6	21	Incremental (4 days)	50–1000 (variable)	50–100 (variable)	-	-

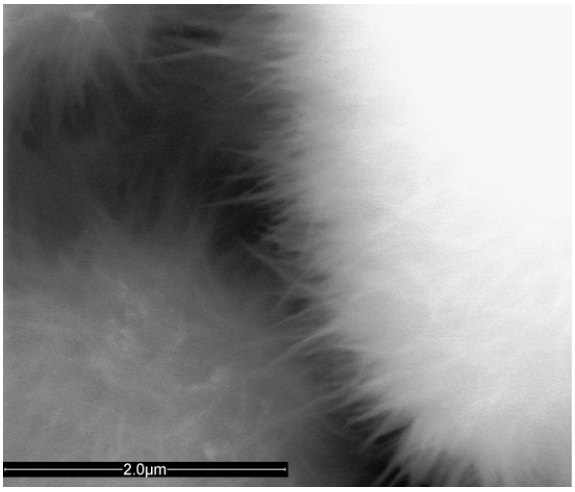

Fig. 1. Sample 1: Micrograph of an oven-dried C_3S paste imaged at 33% RH. The C–S–H product in this image presents a fine needlelike morphology.

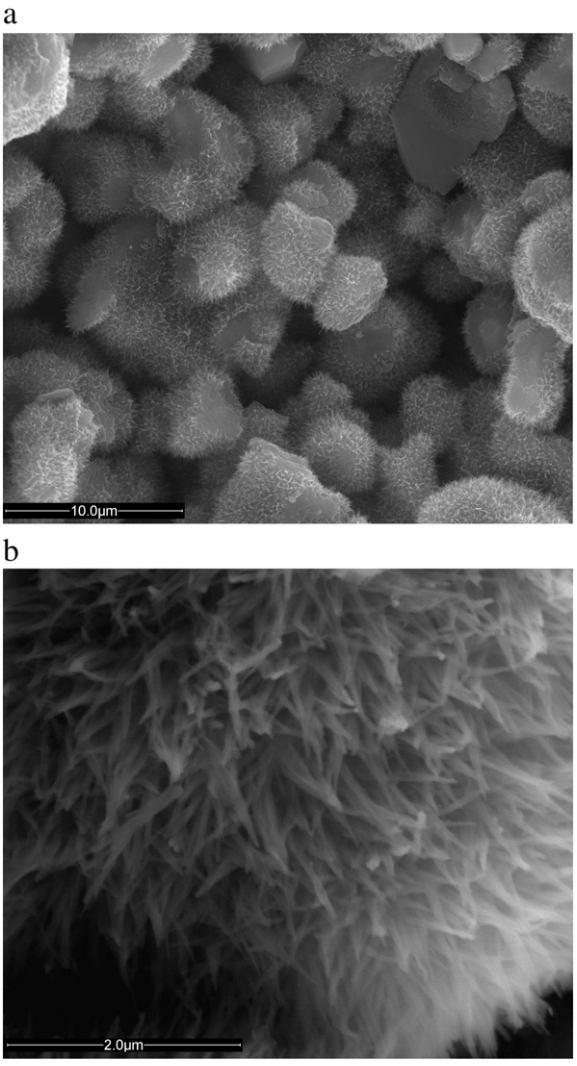

Fig. 2. Sample 2: Micrographs of C_3S paste hydrated for 3 days before rapidly drying from 100% RH to 33% RH in the ESEM. (a) Several C_3S particles encased in C–S–H at a relatively low magnification. (b) Higher magnification of a fibrillar structure of C–S–H. The C–S–H product in this sample presents a fibrillar structure similar to the oven-dried sample (Sample 1), except that Sample 2 has thicker needles.

presents an amorphous morphology typical of an incrementally dried younger sample.

The micrographs show a trend that, in early-age C_3S paste samples, a distinct fibrillar structure of C–S–H emerges when the samples were subjected to higher rates of drying. In contrast, slower drying rates produce a microstructure that is less distinct, as observed in the ESEM. Based on these results, it follows that, to some degree, the morphology of C–S–H may be a consequence of drying rate. Because the internal volume of large concrete structures does not experience high rates of drying similar to Samples 1–3 and Sample 5, an early-age C–S–H product may more closely resemble the amorphous morphology shown in the incrementally dried specimen in Fig. 4.

3.2. Resolution of features

When drying C_3S paste in the ESEM, very few microstructural changes are shown below 80% RH. We also know that irreversible shrinkage in cement paste occurs when the samples are subjected to environments between 50% and 100% RH. This shrinkage must correspond to at least some of the microstructural changes observed here.

Consider the smallest features resolved by the ESEM to explain this phenomenon. At best, one can resolve features that are roughly 10 nm in size. This pore size is approximately the size of the largest gel pores. Using Kelvin's equation

$$ln\frac{p}{p_o} = \frac{2\gamma V_m}{rRT} \quad (1)$$

where p/p_o is the partial pressure, γ=0.0728 N/m is the surface tension, V_m= 1.802E-5 m^3/mol is the molar volume, R= 8.314 Nm/Kmol is the universal gas constant, r is the radius of a pore, and T is the temperature, and substituting T = 278.15 K (5°C) into (1), we can calculate that pores greater than 10 nm in diameter are empty at partial pressures on or below 77%. This condition would explain why few changes are visible in the microstructure when lowering the partial pressure below 80%. Furthermore, because it is not currently possible in the FEI Quanta ESEM to see morphological changes in C–S–H at resolutions better than 10 nm (at low vacuum), the fine nanostructure in its natural state cannot be directly seen.

3.3. Older samples and the mechanism of morphology formation

The trend that rapid drying rates produce a fibrillar C–S–H morphology whereas slower drying rates produce a more amorphous morphology is not replicated in mature samples. As shown in Fig. 6, the experiment cannot be reproduced for incrementally dried C_3S paste specimens approximately 21 days into hydration. Instead, these specimens show a mixed result, with about 50% of the image presenting a fibrillar morphology, and the rest with an amorphous morphology typical of an incrementally dried younger sample. At this point, the fibers shown may have naturally formed. These observations support a mechanism where colloidal particles condense and rearrange into different morphologies [34] [35]. Jennings has proposed a model of C–S–H as an aggregation of precipitated colloidal particles [36] with a similar mechanism. In this model, during the early stages of reaction, nanoscale C–S–H particles loosely pack but rearrange and condense during drying. The mixed morphology of older incrementally dried C_3S paste specimens suggests that, during hydration, a fibrillar product may naturally form (i.e. without drying), particularly in the more open regions.

3.4. Irreversible changes to the C–S–H morphology

We hypothesize that an irreversible change occurs during rapid drying and that these changes are most dramatic at early ages. To

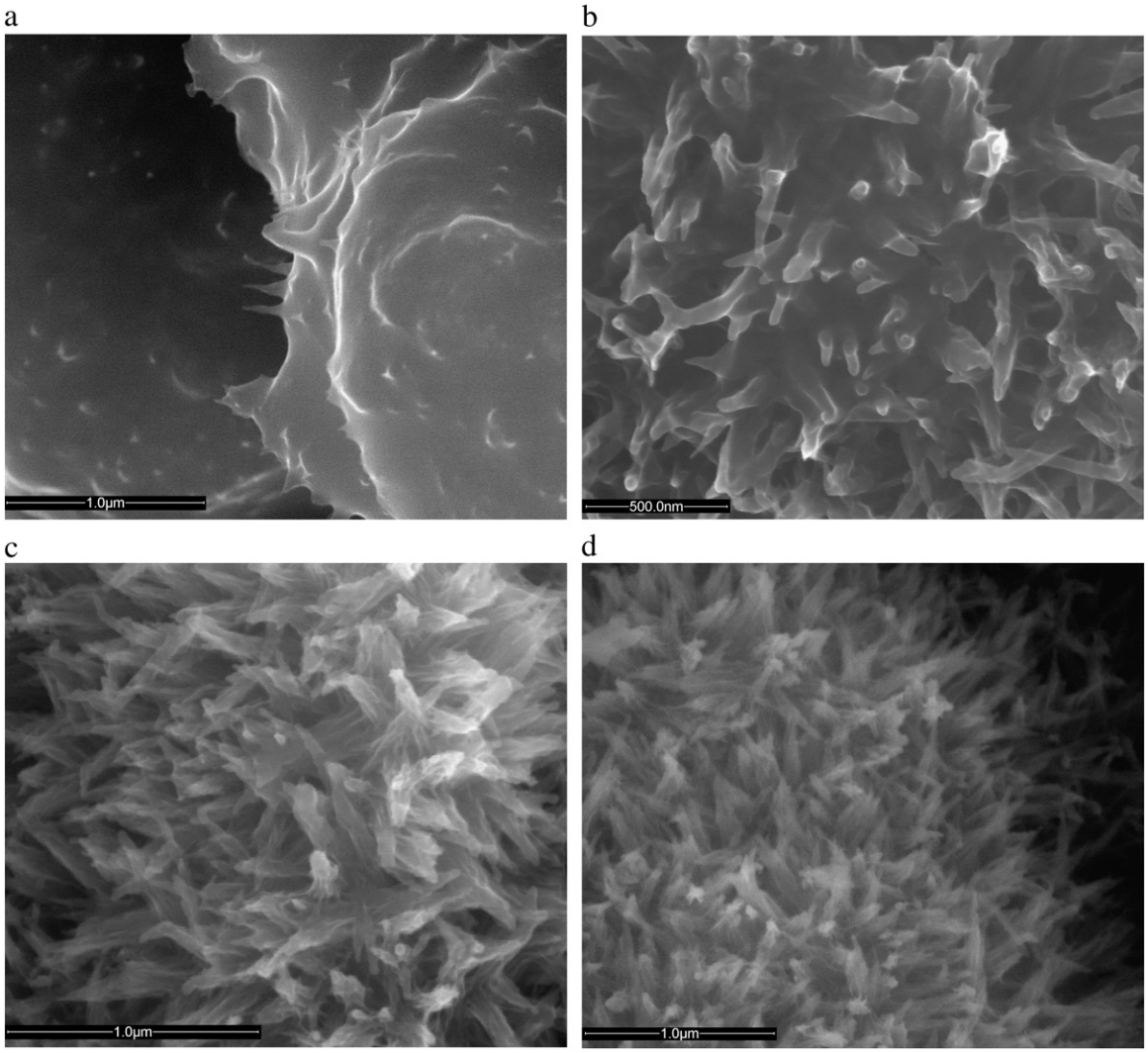

Fig. 3. Sample 3: Micrographs of C_3S paste hydrated for 3 days before drying for 2 hours in the ESEM. Approximate partial pressures are (a) 100% RH, (b) 88% RH, (c) 75% RH, and (d) 33% RH. Note that much of what is shown in (a) is bulk water. The fibrillar C–S–H product in (c) and (d) has a greater thickness compared to the needles/fibers in Samples 1 and 2.

support this hypothesis, many specimens were rewet after the first drying by raising the pressure in the ESEM chamber to vapor pressure. The beam was then switched off to allow the samples to reabsorb water for 1 hour without incurring further radiation damage. As expected, we saw mostly bulk water at partial pressures greater than 95%. However, at about 90% RH, we could see the fine fiber morphology typically seen at around 80% RH during the first drying cycle. In general, the greatest changes in microstructure were perceived between 80% and 90% RH during first drying and between 85% and 90% RH during second drying. Although this difference is small, this trend was observed several times. This observation suggests that irreversible changes to the morphology of C–S–H occur during first drying.

In one experiment, a C_3S paste sample with 0.5 w/c was prepared and wet cured in a lime water solution for 3 days. The sample was then broken in half. One half (Sample 7) was immediately placed back in lime water, and the second half (Sample 8) was placed in a 76% RH desiccator (purged with nitrogen gas). After approximately 16 hours, the second half was resaturated in the lime water before imaging in the ESEM. Fig. 7 is a comparison of Samples 7 and 8 at approximately 85%–90% RH. As with samples that were rewet in the ESEM chamber, we can easily see the fibers in Sample 8. Sample 7 eventually formed fibers similar to those in Fig. 7(b) at 80% RH (not shown). The evidence suggests that the formation of a fibrillar morphology is irreversible.

Typically, we cannot observe the interior hydration product on a specimen's fracture surface. However, there is evidence to suggest that drying at high relative humidity does not affect the interior C–S–H product as much as it does the exterior product. In one study, Neubauer *et al.* used ESEM and drying shrinkage models to show that the outer/LD C–S–H product shrinks upon drying to 80% RH whereas the inner/HD product does not [17]. Therefore, it is possible that the inner/HD product does not also change in morphology at partial pressures higher than 80% RH, regardless of the drying rate. However, because the interior product is not directly observed on a fracture surface, we do not draw direct conclusions on its change in morphology due to drying rate in this paper.

3.5. Changes in surface area

Historically, BET measurements are made using either nitrogen or water vapor as the sorptive gas. The resulting surface area, which differs between the two gases, was the subject of vigorous debate in the 1960s and 1970s. The surface area obtained using water vapor is typically consistent at 200 m^2/g [5], whereas the same measurement using nitrogen is usually much lower and more variable. The discrepancy between nitrogen and water vapor BET measurements could be explained by the inaccessibility of nitrogen to the inner/HD product due to its larger molecular size [10] [9].

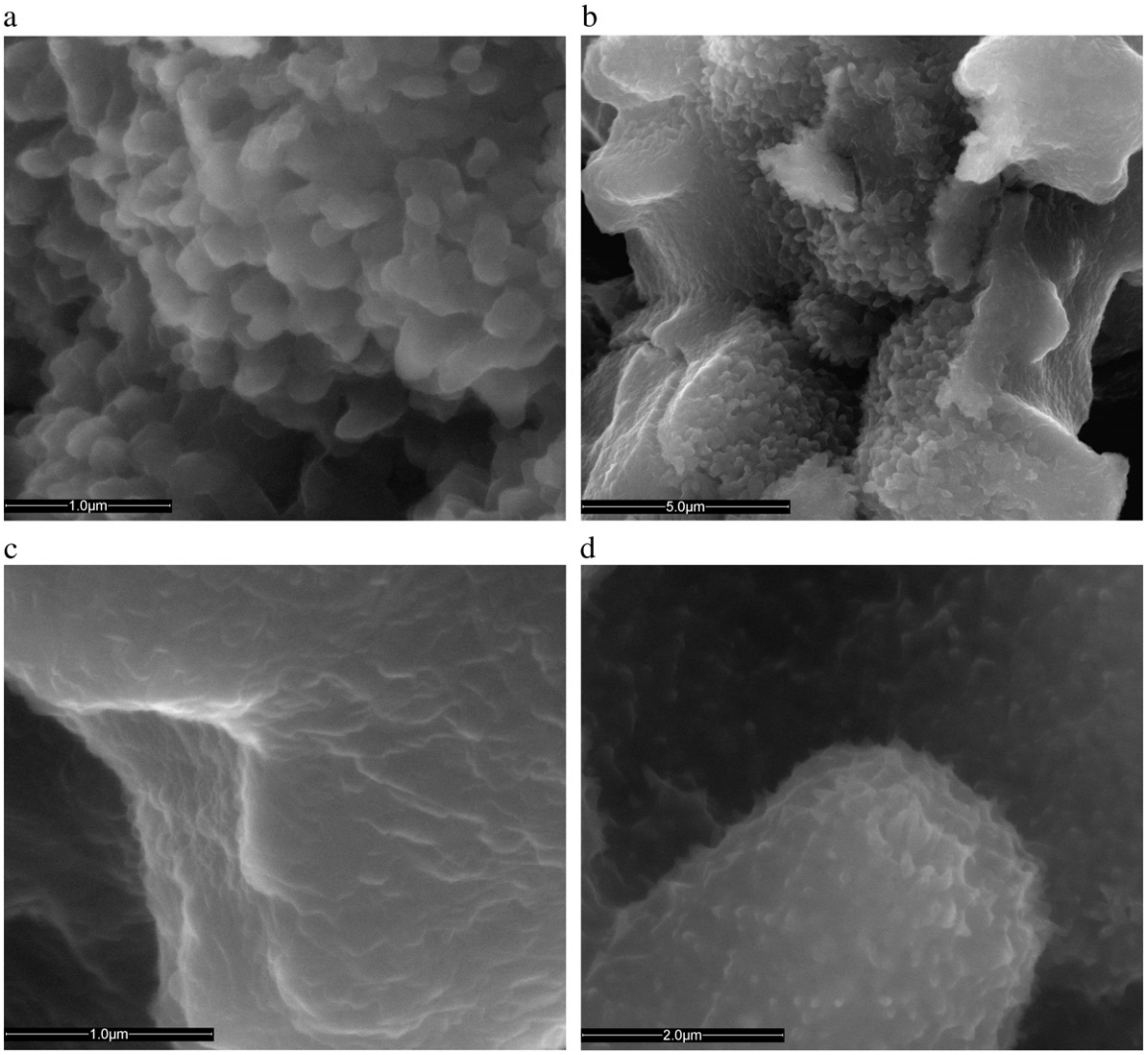

Fig. 4. Sample 4: Micrographs of C_3S paste that was hydrated for 3 days and then incrementally dried for 18 days in desiccators flushed with nitrogen gas to limit CO_2 exposure. The partial pressure is 75% in (a)–(c) and 33% in (d). Here, the C–S–H morphology demonstrates a mixed bumpy and amorphous morphology, and the fibrillar or needlelike product shown in more rapidly dried paste is absent.

Since Hunt's BET experiment in the 1960s (see the Introduction), other researchers have compared the effect of different drying techniques on cement surface area. In the 1970s, Litvan compared the effect of P-drying, D-drying, and oven drying on nitrogen BET measurements for Portland cement paste [20]. Progressively higher surface areas corresponded to harsher drying conditions as a result. More recently, Korpa and Trettin have performed a similar experiment, resulting in a similar trend between the P-drying and D-drying methods, but reported a comparatively lower surface area for oven-dried specimens [37]. Oven drying is typically considered the most damaging drying method among the three [38]. One explanation is that oven drying causes a collapse of the interlayer pores, resulting in lower surface area measurements.

Estimates of the surface areas for Samples 1–5 are compared and summarized in Table 2. The calculation was made by estimating the surface area, volume, and mass of one C–S–H needle, fibril, or bump, using a density of 2.3 g/cc [39]. Note that this surface area was taken from the C–S–H exterior, as shown in the micrographs in Figs. 1–5. The results show a modest increase in surface area with harsher drying conditions, a trend that is in partial agreement with Korpa and Trettin and in full agreement with Litvan and Hunt. An increase in surface area may therefore correlate to greater changes to the C–S–H morphology on drying.

4. Conclusion

Micrographs of C_3S paste samples subjected to various drying rates were taken to examine morphological changes in C–S–H microstructure. These micrographs were taken with an ESEM under specified temperature and pressure conditions so that the relative humidity of the environment around the specimens could be controlled. Every effort was made to minimize carbonization and beam damage. The mechanism(s) of formation of the various morphologies are not well understood, and although this type of microscopic observation cannot prove a mechanism, it can shed light on the possibilities. In this spirit, we interpret the results as follows.

1. *The C–S–H morphology in early-age C_3S paste is more affected by drying rate at high relative humidity (greater than 85%) than by the level of relative humidity*. In early-age specimens subjected to rapid drying rates, C–S–H appeared fibrillar, a morphology observed by previous investigators. In specimens that were very slowly dried, the morphology was less distinct in early-age specimens. The sensitivity to drying rate was most apparent at partial pressures greater than 85%. Older rapidly dried samples also tended to show a fibrillar morphology, but older slowly dried specimens tended to present a mixed fibrillar and amorphous

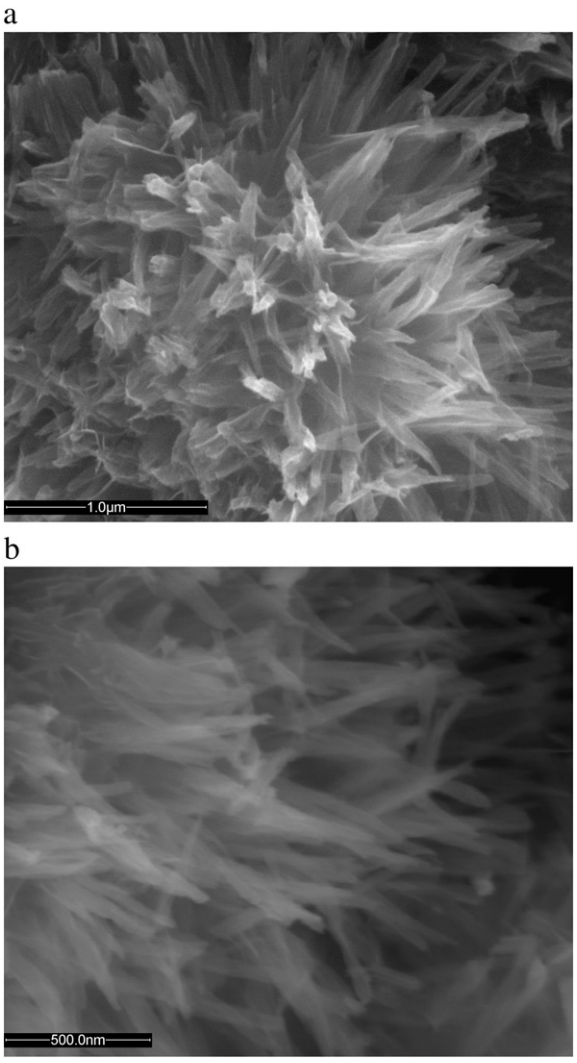

Fig. 5. Sample 5: Micrographs of C_3S paste hydrated for 21 days and imaged at (a) 75% RH and (b) 33% RH. The presence of a fibrillar C–S–H product is similar to that of a young C_3S paste but is unlike the amorphous morphology shown in an incrementally dried specimen (i.e., Sample 4). These results indicate that the C–S–H morphology is more dependent on drying rate rather than time after curing.

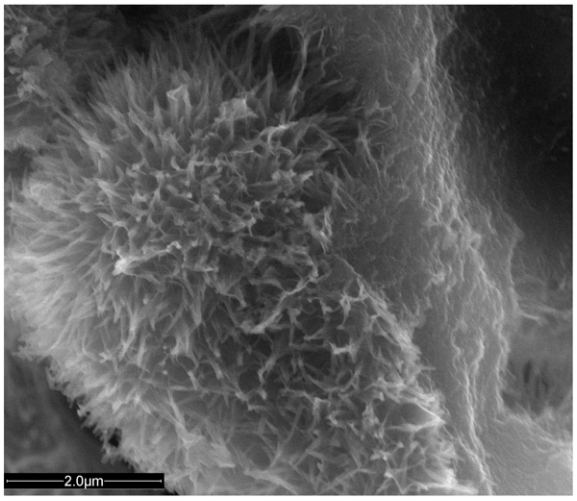

Fig. 6. Sample 6: Micrograph of C_3S paste hydrated for 21 days, incrementally dried to 75% RH, and imaged at 75% RH. In this image, both fibrillar and amorphous C–S–H morphologies are shown. The morphology in this specimen suggests that, over time, fibers may naturally form in wet cured C_3S paste.

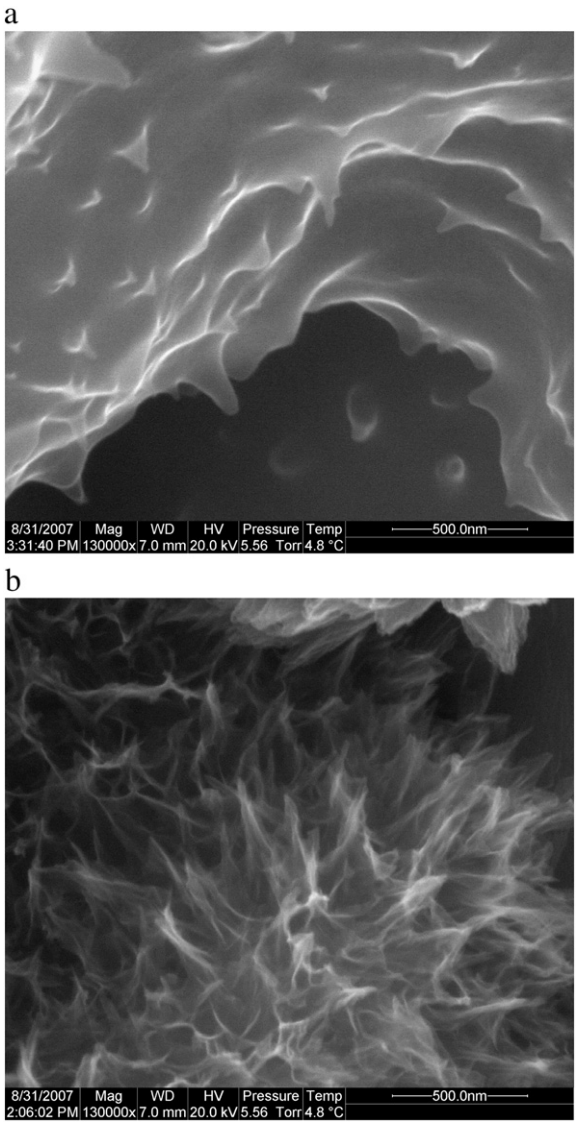

Fig. 7. Samples 7 and 8: Comparison of microstructure at (a) first drying (Sample 7) and (b) second drying (Sample 8) at the same temperature and pressure (approximately 85%–90% RH). The fibrillar C–S–H morphology more quickly emerges in a previously dried C_3S paste specimen.

structure, an observation that suggests that a fibrillar product may naturally form over time.

2. *The morphology of C–S–H cannot yet be imaged in its natural state.* ESEM micrographs are limited to a resolution of approximately 10 nm at best. Kelvin's equation predicts that all pores below 10 nm in diameter are empty below 77% partial pressures. Consequently, changes in the microstructural features of C–S–H in its natural state, particularly with regard to gel pores less than 10 nm, cannot currently be seen in an ESEM.

Table 2
Estimation of LD (External) Surface Area at 33% RH.

Sample number	Age (days)	Drying method	Surface area per unit mass (nm^2)
1	3	Oven	109
2	3	Rapid	70
3	3	Slow (2 hrs)	35
4	3	Incremental (18 days)	18
5	21	Rapid	39
6	21	Incremental (4 days)	Mixed results

3. *External surface area increases with harsher drying conditions*. Surface area calculations for the external C–S–H product were estimated for each sample, showing that, as the rate of drying increased, so did the outer surface area of C–S–H. These results follow a similar trend of the literature values of BET nitrogen sorption measurements of cement paste subjected to various drying conditions.
4. *C–S–H has properties similar to gels*. One characteristic of a gel is that greater changes in morphology are caused by the gradient of capillary pressure. These gradients develop due to the rate of drying. As shown in micrographs of C_3S paste at early ages, the morphology of the C–S–H hydration product markedly changes with higher drying rates, giving C–S–H one of the important properties of a gel. These observations suggest that the needles and other morphologies that naturally form over time are accelerated by rapid drying and are interrupted by slow drying.

Acknowledgments

This work was funded in part by the National Science Foundation under Contract CMS 0409571. The ESEM micrographs were taken in the Electron Probe Instrumentation Center (EPIC), a facility of the Atomic and Nanoscale Characterization Experimental (NUANCE) Center at Northwestern University. NUANCE is supported in part by NSF–Nanoscale Science and Engineering Center (NSEC), NSF–Materials Research Science and Engineering Centers (MRSEC), Keck Foundation, the State of Illinois, and Northwestern University.

References

[1] H. Taylor, Cement Chemistry, 2nd EditionThomas Telford Services Ltd, London, 1997.
[2] G. Scherer, Structure and properties of gels, Cem. Concr. Res. 29 (1999) 1149–1157.
[3] J. Thomas, H. Jennings, A colloidal interpretation of chemical aging of the C-S-H gel and its effects on the properties of cement paste, Cem. Concr. Res. 36 (2006) 30–38.
[4] T. Powers, T. Brownyard, Studies of the physical properties of hardened Portland cement paste, Bull., 22, Portland Cement Association, Chicago, IL, 1948, p. 992, 43.
[5] T. Powers, Structure and physical properties of hardened Portland cement paste, J. Amer. Cer. Soc. 41 (1) (1958) 1–6.
[6] J. Taplin, A method for following the hydration reaction in Portland cement paste, Australian Journal of Applied Science.
[7] S. Diamond, Cement paste microstructure: An overview at several levels, in: Hydraulic Cement Pastes: Their Structure and Properties, Proc. Symp, Cement and Concrete Association (1977) 2–31.
[8] H. Jennings, B. Dalgleish, P. Pratt, Morphological development of hydrating tricalcium silicate as examined by electron microscopy techniques, J. Am. Ceram. Soc. 64 (10) (1981) 567.
[9] H.M. Jennings, A model for the microstructure of calcium silicate hydrate in cement paste, Cem. Concr. Res. 30 (2000) 101.
[10] P. Tennis, H. Jennings, A model for two types of calcium silicate hydrate in the microstructure of Portland cement pastes, Cem. Concr. Res. 30 (2000) 855–863.
[11] M. Diamon, S. Ueda, R. Kondo, Morphological study on hydration of tricalcium silicate, Cem. Concr. Res. 1 (1971) 391–401.
[12] I. Richardson, Tobermorite/jennite- and tobermorite/calcium hydroxide - based models for the structure of C–S–H: Applicability to hardened pastes of tricalcium silicate, Portland cement, and blends of Portland cement with blast-furnace slag, metakaolin, or silica fume, Cem. Concr. Res. 34 (2004) 1733.
[13] I. Richardson, The nature of C–S–H in hardened cements, Cem. Concr. Res. 29 (1999) 1131–1147.
[14] R. Williamson, Solidification of Portland cement, Prog. Mater. Sci. 15 (3) (1972) 189–286.
[15] S.U.M. Daimon, R. Kondo, Morphological study on hydration of tricalcium silicate, Cem. Concr. Res. 1 (1971) 391.
[16] C. Neubauer, H. Jennings, The role of the environmental scanning electron microscope in the investigation of cement-based materials, Scanning 18 (1996) 515–521.
[17] C. Neubauer, T. Bergstrom, K. Sujata, Y. Xi, E. Garboczi, H. Jennings, Drying shrinkage of cement paste as measured in an environmental scanning electron microscope and comparison with microstructural models, J. Mat. Sci. 32 (1997) 6415–6427.
[18] J. Thomas, A. Allen, H. Jennings, Structural changes to the calcium–silicate–hydrate gel phase of hydrated cement with age, drying, and resaturation, J. Am. Cer. Soc. 91 (10) (2008) 3362–3369.
[19] C. Hunt, Nitrogen sorption measurements and surface areas of hardened cement pastes, Highw. Res. Board.
[20] G. Litvan, Variability of the nitrogen surface area of hydrated cement paste, Cem. Concr. Res. 6 (1976) 139–144.
[21] J.J. Thomas, H.M. Jennings, A.J. Allen, The surface area of cement paste as measured by various techniques, Concr. Sci. Eng. 1 (1999) 45.
[22] G. Scherer, Drying gels: VIII. Revision and review, J. Non-Crystalline Solids 109 (1989) 171–182.
[23] J. S. Gevrenov, Microstructure and drying shrinkage of ordinary Portland cement and alkali-activated slag pastes as a function of relative humidity, Master's thesis, Northwestern University (2005).
[24] D. Double, Some studies of the hydration of Portland cement using high-voltage (1-MV) electron microscopy, Mat. Sci. En0067. 12 (1973) 29–32.
[25] D. Double, A. Hellawell, S. Perry, The hydration of Portland cement, Proc. R. Soc. Lond. A. 359 (1978) 435–451.
[26] H. Jennings, P. Pratt, The use of a high-voltage electron microscope and gas reaction cell for the microstructural investigation of wet Portland cement, J. Mater. Sci. 15 (1) (1980) 250–253.
[27] D. Silva, P. Monteiro, The influence of polymers on the hydration of Portland cement phases analyzed by soft X-ray transmission microscopy, Cem. Concr. Res. 36 (2006) 1501–1507.
[28] D. Silva, P. Monteiro, Hydration evolution of C_3S–EVA composites analyzed by soft X-ray microscopy, Cem. Concr. Res. 35 (2005) 351–357.
[29] A. Zingg, L. Holzer, A. Kaech, F. Winnefeld, J. Pakusch, S. Becker, L. Gauckler, The microstructure of dispersed and nondispersed fresh cement pastes—New insight by cryomicroscopy, Cem. Concr. Res. 38 (2008) 522–529.
[30] B. Möser, J. Stark, A new model of ordinary Portland cement hydration derived by means of ESEM–FEG, in: A. Boyd, S. Mindess, J. Skalny (Eds.), Materials Science of Concrete: Cement and Concrete—Trends and Challenges, The American Ceramic Society, Westerville, Ohio, 2002, pp. 89–107.
[31] D. Double, New development in understanding the chemistry of cement hydration, Phil. Trans. R. Soc. Lond A 310 (1983) 53.
[32] A. J. Allen, J. J. Thomas, H. M. Jennings, Composition and density of nanoscale calcium-silicate-hydrate in cement, Nature 6 (311–316).
[33] K. Snyder, D. Bentz, Suspended hydration and loss of freezable water in cement pastes exposed to 90 percent relative humidty, Cem. Concr. Res. 34 (11) (2004) 2045–2056.
[34] V. Manoharan, M. Elsesser, D. Pine, Dense packing and symmetry in small clusters of microspheres, Science 301 (2003) 483–487.
[35] E. Lauga, M. Brenner, Evaporation-driven assembly of colloidal particles, Phys. Rev. Lett. 93 (2004) 238301.
[36] H. Jennings, Colloid model of C–S–H and its implications to the problem of creep and shrinkage, Mater. Struct. 37 (265) (2004) 59–70.
[37] A. Korpa, R. Trettin, The influence of different drying methods on cement paste microstructures as reflected by gas adsorption: Comparison between freeze-drying (F-drying), D-drying, P-drying, and oven drying methods, Cem. Concr. Res. 36 (2006) 634–649.
[38] C. Gallé, Effect of drying on cement-based materials pore structure as identified by mercury intrusion porosimetry: A comparative study between oven-, vacuum-, and freeze-drying, Cem. Concr. Res. 31 (10) (2001) 1467–1477.
[39] H.M. Jennings, Refinements to colloid model of C–S–H in cement: CM-II, Cem. Concr. Res. 38 (3) (2007) 275–289.